THE ASTROPHYSICAL JOURNAL, 492:379–389, 1998 January 1


# THE SEISMOLOGY OF SUNSPOTS: A COMPARISON OF TIME-DISTANCE AND FREQUENCY-WAVENUMBER METHODS[1]

T. J. BOGDAN, D. C. BRAUN,[2] AND B. W. LITES
High Altitude Observatory, National Center for Atmospheric Research,[3] P.O. Box 3000, Boulder, CO 80307-3000

AND

JOHN H. THOMAS[4]
Department of Mechanical Engineering, Department of Physics and Astronomy, and C. E. K. Mees Observatory, University of Rochester, Rochester, NY 14627
*Received 1997 April 4; accepted 1997 August 13*

## ABSTRACT

A pair of formulae are developed that relate the absorption coefficient and partial-wave phase shift concepts of frequency-wavenumber local helioseismology to the center-annulus cross-correlation function of time-distance helioseismology, under the general circumstances that both induced and spontaneous sunspot oscillations may be present. These formulae show that spontaneous emission of *p*-modes by magnetic and Reynolds stresses within the spot and the mode mixing between incoming and outgoing *p*-modes affect only the outgoing center-annulus cross-correlation time $\tau^+$, and they caution that real or spurious phase lags of the umbral oscillation signal lead to differences in the incoming and outgoing correlation times, resulting in $\tau^- \neq \tau^+$. The application of these methods to actual helioseismic data obtained by the Global Oscillation Network Group (GONG) project is carried out in order to provide a tangible illustration of how time-distance and frequency-wavenumber ideas can profitably be combined to yield deeper insight into the seismic probing of sunspots.

By using the helioseismic GONG data in conjunction with concurrent observations of Doppler velocities and vector magnetic fields obtained by the High Altitude Observatory/National Solar Observatory (HAO/NSO) Advanced Stokes Polarimeter (ASP) for the 1995 October disk passage of active region NOAA 7912, we demonstrate that the inferred GONG umbral signal actually originates from the umbra-penumbra boundary about 6 Mm distant from the center of the spot. Further, the ASP observations show that the 5 minute oscillations at the umbra-penumbra boundary lag behind those in the center of the umbra by approximately 1 minute, which is precisely the difference between the incoming and outgoing correlation times for NOAA 7912 recently determined by Braun. This remarkable result underscores the perils of using umbral oscillations in time-distance helioseismology, and it calls into question previous claims that correlation time differences constitute direct evidence for the existence of a steady downflow in and around sunspots. Taken together, the observational and theoretical evidence suggest that the *p*-mode forcing of the spot leads to the generation of upwardly propagating slow magnetoatmospheric waves. These waves are in turn responsible for the decreased amplitudes of the outwardly propagating *p*-modes in the surrounding quiet Sun, and the dispersion in their travel times between the hidden subsurface layer where they are forced and the overlying level where the Doppler signals originate leads to the observed phase lag between the umbral and penumbral oscillations and the corresponding correlation time differences.

*Subject headings:* Sun: magnetic fields — Sun: oscillations — sunspots

## 1. INTRODUCTION

There are, at present, two distinct formalisms for pursuing the local helioseismology of isolated solar surface features such as sunspots and active regions. The frequency-wavenumber approach, pioneered by Braun and collaborators (Braun, Duvall, & LaBonte 1988; Braun, LaBonte, & Duvall 1990; Braun et al. 1992; Bogdan et al. 1993; Braun 1995), effects a Fourier-Hankel decomposition of the solar acoustic oscillations in an annular domain surrounding the target structure by computing the complex amplitudes of inwardly and outwardly propagating *p*-modes as a function of frequency and horizontal wavenumber (or equivalently, spherical harmonic degree). The robust result of this analysis is a tendency for the outwardly propagating waves to show a reduction in amplitude and a positive phase shift relative to their inwardly propagating counterparts. Both of these trends become more pronounced with the increase of frequency and degree along each *p*-mode ridge, with maximal phase shifts approaching $+150°$ and amplitude reductions as large as 30% relative to the inwardly propagating waves. The time-distance approach, developed by Duvall and coworkers (Duvall et al. 1993; Duvall 1995; Korzennik, Noyes, & Ziskin 1995; D'Silva & Duvall 1995; Duvall et al. 1996; D'Silva et al. 1996; Kosovichev 1996; Braun 1997), determines the temporal cross-correlation function between the time series of intensity or Doppler fluctuations recorded in the sunspot umbra and the azimuthally averaged time series at an

[1] This work utilizes data obtained by the Global Oscillations Network Group (GONG) project, managed by the National Solar Observatory, a Division of the National Optical Astronomy Observatories, which is operated by AURA, Inc., under a cooperative agreement with the National Science Foundation.

[2] Also Solar Physics Research Corporation, 4720 Calle Desecada, Tucson, AZ 85718.

[3] The National Center for Atmospheric Research is sponsored by the National Science Foundation.

[4] Affiliate Scientist, HAO/NCAR.

angular distance $\Delta$ in the surrounding quiet Sun. From these cross-correlation functions, one then determines a pair of positive and negative correlation times associated with the maxima in the envelope and the phase as a function of the angular separation $\Delta$. The persistent result of this analysis is a tendency for the mean of the positive and negative correlation times, $\bar{\tau} = \frac{1}{2}(\tau^+ + \tau^-)$, to be shorter by approximately one-half minute than the analogous mean time obtained when the process is repeated without a sunspot being present, and for the appearance of negative time differences, $\delta\tau = (\tau^+ - \tau^-)$, of order 1 minute, which are not observed for the control experiment in which the sunspot is absent.

Although these observational facts are by now fairly well established, the physical interpretations of what they imply about the structure of the sunspot belong more to the realm of speculation and conjecture. The underlying cause of this situation can be traced directly to the difficulties encountered in solving the relevant linearized wave equations in laterally structured, vertically stratified, and inhomogeneously magnetized plasmas. Consequently, theoretical studies have generally pursued one of two possible options: either overly simplified models have been investigated, affording an exact treatment of the governing equations; or realistic equilibria are retained, but an approximate treatment of the equations is applied. An example of the former approach is the series of papers that attribute the diminished outwardly propagating wave amplitudes to the conversion of *p*-modes to slow magnetoatmospheric waves within the sunspot proper (Spruit 1991; Spruit & Bogdan 1992; Cally & Bogdan 1993; Cally, Bogdan, & Zweibel 1994; Bogdan et al. 1996). The latter approach is represented by a growing body of work based upon ray-tracing techniques that attributes negative time differences $\delta\tau$ to steady flows around the spot (D'Silva & Duvall 1995; Duvall et al. 1996; D'Silva et al. 1996; Kosovichev 1996; Duvall et al. 1997; Kosovichev & Duvall 1998) or based on the use of the Born approximation to infer that the measured positive phase shifts imply that the sunspot acts as a fairly shallow ($\approx$1 Mm) region of increased effective sound speed (Fan, Braun, & Chou 1995; Chou et al. 1996).

The aim of the present contribution is to carry further the efforts begun by Bogdan (1997) to quantify the relationship between the time-distance and frequency-wavenumber approaches to local helioseismology. In Bogdan (1997), the correspondence between the treatment of *p*-mode propagation in terms of ray bundles and as a superposition of normal modes was investigated for a homogeneous stratified atmosphere. Here we allow for the presence of a magnetic inhomogeneity (sunspot) capable of scattering and absorbing the incident acoustic oscillations, in addition to emitting *p*-modes it generates through its own internal magnetic and Reynolds stresses. It was shown by Bogdan (1997) that an accurate assessment of the interaction of stochastically excited *p*-modes with such a target structure requires either a superposition of many neighboring ray paths to form an extended[5] ray bundle or a superposition of numerous global modes of oscillation to form a wave packet. The second approach is pursued in §§ 2 and 3, where we determine the explicit dependence of the center-annulus cross-correlation function employed in time-distance helioseismology upon the incoming and outgoing mode amplitudes and phase shifts measured through frequency-wavenumber local helioseismology. The resulting formulae, embodied by equations (10), (11), (12), and (13) below, are particularly illuminating in demonstrating a close connection between the mean correlation time $\bar{\tau}$ and the attendant mode mixing between incoming and scattered *p*-modes across radial orders at fixed frequency and in showing that the time difference $\delta\tau$ is extremely sensitive to nuances of the (inferred) umbral oscillations.

In § 4, these points are illustrated through the comparison of time-distance and frequency-wavenumber analyses as applied to the 1995 October disk passage of active region NOAA 7912. This comparison is aided dramatically by the use of concurrent observations obtained with the High Altitude Observatory/National Solar Observatory (HAO/NSO) Advanced Stokes Polarimeter (ASP) and with the Global Oscillation Network Group (GONG) instruments. The remarkable outcomes of the comparison of these two sets of data are the discoveries that the GONG umbral oscillation signal in fact comes from the inner edge of the sunspot penumbra and that there is a time lag comparable to the observed $\delta\tau$ between the oscillations at the inner edge of the penumbra and the center of the umbra. The continuum-intensity contrast at $\lambda \approx 630$ nm between these two locations is approximately 3:1, so given the $\approx 9''$ size of the GONG pixels, it is not unreasonable that scattered penumbral light contaminates the oscillation signal in the GONG pixel(s) identified with the umbra of the sunspot.

This finding underscores the perils of comparing oscillation signals within the sunspot with those from the surrounding quiet Sun. It also casts serious doubt on the claims made by Duvall et al. (1996) that the observed $\delta\tau \approx 30$ s time difference exhibited by the sunspot center-annulus cross-correlation function can be construed as evidence of a $\approx 2$ km s$^{-1}$ downflow that persists to a depth of 2 Mm below the spot. Such downflows, which are implied by the Parker (1992) model of sunspot formation, may in fact be present in and around sunspots, but it is first necessary to determine the fraction of the measured time difference that results from penumbral contamination in conjunction with the attendant phase lag before ascribing the remainder to some other physical agent, such as steady downflows.

## 2. BASIC THEORY

The basic theoretical treatment of the local helioseismology of sunspots is largely an obvious generalization of the well-known formalism developed to study the nonradial pulsations of spherically symmetric stars (Ledoux & Walraven 1958; Cox 1980, p. 112; Unno et al. 1989). The essential point of departure is the notion of developing a local description of the oscillations within the sunspot and its immediate vicinity. As illustrated by Figure 1, the starting point of the analysis is the specification of a local system of spherical coordinates $(r, \theta, \phi)$ with the polar axis aligned with the center of the sunspot. The region of interest extends out to a maximum polar angle $\theta_{\max} \approx 30^\circ$ that is typically chosen to avoid enclosing other sunspots or active regions within the field of interest. An outer annular region of extent $\theta_> \le \theta \le \theta_{\max}$ can therefore be regarded as containing essentially quiet Sun, and in this region it is appropriate to

[5] The finite spatial and temporal extent of actual solar wave packets is a consequence of the fairly restricted range of frequencies and wavenumbers of the detected modes of oscillation, and in particular, of the absence of oscillations with vary large radial orders $n \gg 1$ that are commonplace in ocean acoustics.

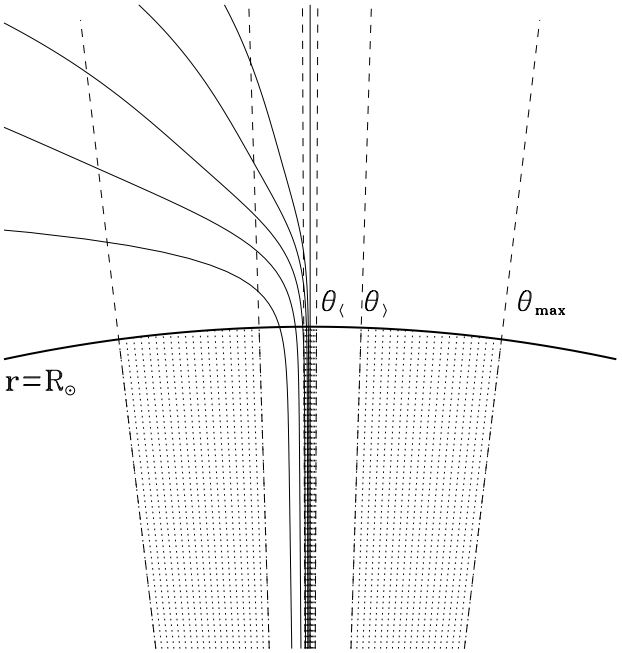


FIG. 1.—Sketch of the local spherical coordinate system centered on the umbral axis of an isolated sunspot. Only half of the magnetic field lines are drawn and the structure is assumed to be axisymmetric. Polar angles $\theta_<$, $\theta_>$, and $\theta_{max}$ delineate the boundaries of the shaded regions where the inner and outer expansions of § 2 are valid.

express the Lagrangian fluid displacement as a separable superposition of eigenmodes,

$$\delta \boldsymbol{r}^{>}(\boldsymbol{r}, t) = \mathrm{Re}\left\{\sum_{nlm} e^{i\omega_{nl}t} \times \left[\xi_{nl}^{>}(r),\ \eta_{nl}^{>}(r)\frac{\partial}{\partial\theta},\ \eta_{nl}^{>}(r)\frac{1}{\sin\theta}\frac{\partial}{\partial\phi}\right]^T \times \left[A_{nlm}\, Y_{lm}^{(-)}(\theta, \phi) + B_{nlm}\, Y_{lm}^{(+)}(\theta, \phi)\right]\right\}, \quad (1)$$

where $A_{nlm}$ and $B_{nlm}$ are complex constants and $\xi_{nl}^{>}(r)$ and $\eta_{nl}^{>}(r)$ are the solutions of an appropriate pair of coupled ordinary differential equations that depend upon the radial stratification of the spherically symmetric star. The functions

$$Y_{lm}^{(\pm)}(\theta, \phi) \equiv \sqrt{\frac{2l+1}{16\pi}\frac{(l-m)!}{(l+m)!}} \times \left[P_l^m(\cos\theta) \pm \frac{2i}{\pi} Q_l^m(\cos\theta)\right] e^{im\phi} \quad (2)$$

are the inwardly (−) and outwardly (+) propagating wave components whose superposition forms the standing wave spherical harmonic function $Y_l^m(\theta, \phi)$. The associated Legendre function, $Q_l^m(\cos\theta)$, can safely be employed because its singular behavior at $\theta = 0$ and $\pi$ resides outside of the outer annular region $\theta_> \le \theta \le \theta_{max}$. Equation (1) will certainly fail to converge beyond the polar angle between the spot and its nearest neighbor sunspot, which acts like a coherent point source of (scattered) $p$-modes. A discussion of the linear independence of the terms in the expansion, as well as of optimal strategies for selecting stencils of spherical harmonic degrees employed in the summation, can be found in Bogdan et al. (1993) and Braun (1995).

Equation (1) neglects the presence of surface—or jacket—modes that decline monotonically away from the sunspot boundary into the surrounding quiet Sun (Bogdan & Cally 1995). In the present circumstance, these modes are associated with complex angular degrees $l = -\frac{1}{2} \pm i\rho$ (where $\rho$ is any real number), and an appropriate combination of $Y_{-1/2\pm i\rho,m}^{(\pm)}(\theta, \phi)$ must be employed to generate a conical function that decreases monotonically from $\theta_>$ toward $\theta_{max}$ (i.e., see Lebedev 1972, p. 210). The neglect of the jacket modes can usually be justified on the grounds that they have decayed to fairly low amplitudes for moderate to large values of $\theta$, and, in any case, they do not transport wave energy away from or toward the sunspot. For composite sunspots that are composed of many individual magnetic fibrils, the neglect of the jacket modes in determining the acoustic interactions between the individual fibrils is questionable.

As noted earlier in § 1, the primary difficulty encountered in the theoretical treatment of sunspot seismology is the absence of a separable expansion analogous to equation (1) valid within the sunspot proper. Such an expansion is possible (only?) if the magnetic field is purely radial, $\boldsymbol{B} = B_0\hat{\boldsymbol{e}}_r$, and independent of both latitude and longitude (Cally 1983). It may well be envisaged that these two criteria are approximately satisfied very close to the axis of the sunspot, and so for $0 \le \theta \le \theta_<$ we adopt a separable inner expansion

$$\delta \boldsymbol{r}^{<}(\boldsymbol{r}, t) = \mathrm{Re}\left\{\sum_{\nu\lambda\mu} e^{i\omega_{\nu\lambda}t}\left[\xi_{\nu\lambda}^{<}(r),\ \eta_{\nu\lambda}^{<}(r)\frac{\partial}{\partial\theta},\ \eta_{\nu\lambda}^{<}(r)\frac{1}{\sin\theta}\frac{\partial}{\partial\phi}\right]^T \times C_{\nu\lambda\mu}\, Y_\lambda^\mu(\theta, \phi)\right\}, \quad (3)$$

where the $C_{\nu\lambda\mu}$ are another set of complex constants, different from the $A_{nlm}$ and $B_{nlm}$ encountered above in the outer expansion, equation (1). The appropriate coupled equations for $\xi_{\nu\lambda}^{<}(r)$ and $\eta_{\nu\lambda}^{<}(r)$ may be found in Cally (1983) along with a thorough discussion of their solutions under typical solar conditions. Distinct subscripts $\{\nu\lambda\mu\}$ are employed in equation (3) to emphasize that the oscillation eigenvalue problem within the magnetized umbral atmosphere is distinct from that in the surrounding quiet Sun, and consequently there is no reason to suppose that the two problems will share identical eigenvalue spectra. For example, because of coupling between the fast and slow magneto-atmospheric wave modes and the ability of the latter to propagate along the magnetic field lines into the overlying solar atmosphere and the solar interior, the allowed spherical harmonic degrees $\lambda$ are necessarily complex if the frequencies $\omega_{\nu\lambda}$ are assumed to be real, and vice versa (Bogdan & Cally 1997). Since the inner core of the sunspot umbra is assumed to be axisymmetric, $\mu$, like its outer counterpart $m$, is similarly restricted to integer values.

If there is no sunspot, inhomogeneity, or source of $p$-modes within the region of interest, then $\theta_>$ may be reduced to 0, and $B_{nlm} \to A_{nlm}$. To handle the most general situation, we extend the ideas developed by Braun (1995), and write

$$B_{nlm} = \sum_{n'l'm'} \mathcal{S}_{nlm}^{n'l'm'} A_{n'l'm'} + \sum_{\nu\lambda\mu} \mathcal{T}_{nlm}^{\nu\lambda\mu} A_{\nu\lambda\mu}\,. \quad (4)$$

The first term on the right-hand side of this equation takes account of the induced emission of outgoing $p$-modes that results from the forcing of the spot by the incoming wave

field. By analogy with the quantum mechanical treatment of particle scattering, the set of complex coefficients $\mathcal{S}^{n'l'm'}_{nlm}$ is collectively termed the scattering, or $S$-matrix. The first sum on the right-hand side of equation (4) includes all accessible outgoing $p$-mode channels, which in the present circumstance simply amount to the requirement that $\omega_{nl} = \omega_{n'l'}$, assuming that the sunspot evolves on timescales that are long compared to the characteristic $p$-mode periods. It is customary to rewrite the diagonal elements of the $S$-matrix as

$$\mathcal{S}^{nlm}_{nlm} = \sqrt{1 - \alpha_{nlm}}\, e^{i\delta_{nlm}}\,, \tag{5}$$

in terms of two real numbers $\alpha_{nlm}$ and $\delta_{nlm}$, termed the "absorption coefficient" and the scattering "phase shift," respectively. The off-diagonal elements of the $S$-matrix describe the mode mixing caused by the spot. The basic goal of frequency-wavenumber helioseismology is to determine the $S$-matrix based (exclusively) on knowledge of $\delta \boldsymbol{r}^{>}(R_\odot, \theta, \phi, t)$. When a sunspot is present, the departures of $\alpha_{nlm}$ and $\delta_{nlm}$ from zero and the existence of off-diagonal elements of the $S$-matrix are direct measures of the modification suffered by these oscillations because of the presence of the spot.

The second sum on the right-hand side of equation (4) accounts for the spontaneous emission of outgoing $p$-modes caused by the excitation of umbral oscillations by stresses within the sunspot. The complex constants $A_{\nu\lambda\mu}$ (which are distinct from the incoming $p$-mode amplitudes $A_{nlm}$) give the amplitudes of the umbral oscillations that would be expected in the absence of any incoming $p$-modes from the surrounding quiet Sun. For the inner expansion coefficients, the statement analogous to equation (4) reads

$$C_{\nu\lambda\mu} = A_{\nu\lambda\mu} + \sum_{nlm} \mathcal{U}^{nlm}_{\nu\lambda\mu} A_{nlm}\,, \tag{6}$$

where the two terms on the right-hand side of this equation represent the spontaneous and induced umbral oscillations, respectively. The coupling between the incident wave field and the induced umbral oscillations is quantified by a $U$-matrix, following the notation introduced by Abdelatif & Thomas (1987), while the $T$-matrix of equation (4) connects the spontaneous umbral oscillations to the outgoing $p$-mode wave field. The sums that contain the $T$- and $U$-matrices are restricted to pairs of umbral and quiet-Sun oscillation modes for which $\mathrm{Re}\,(\omega_{\nu\lambda}) = \omega_{nl}$ or $\mathrm{Re}\,(\omega_{\nu\lambda}) = \omega_{n'l'}$, and $|\,\mathrm{Im}\,(\omega_{\nu\lambda})| \ll \mathrm{Re}\,(\omega_{\nu\lambda})$.

It is worth reiterating that if the magnetic inhomogeneity is absent, then $\theta_<$ can be increased to $\theta_{\max}$, $C_{\nu\lambda\mu} \to A_{nlm}$, and the radial umbral eigenfunctions become identical to their quiet-Sun counterparts. In this case, the outer and inner expansions, equations (1) and (3), have a region of common overlap. In general, however, a real sunspot is dominated by $B_\theta$ fields in its penumbra, and sensible $B_\theta$ fields are present well into the central portions of the umbra. Thus $\theta_<$ is likely to be very small in practice and certainly to be bounded well away from $\theta_>$, prohibiting the overlap of the two expansions. The lack of a common region of validity for the expansions equations (1) and (3) is the primary complication encountered in the theoretical treatment of sunspot seismology.

In summary, for any particular realization of the local wave field in the vicinity of a sunspot, there exist two unique sets of complex amplitudes $A_{\nu\lambda\mu}$ and $A_{nlm}$ that describe oscillations that have their origin inside and outside, respectively, of the spot. The additional oscillations that result from the presence of the spot are determined by the action of the $S$-, $T$-, and $U$-matrices on these complex mode amplitudes, as explicitly indicated by equations (4) and (6). The measurement of the complex mode amplitudes $A_{nlm}$, $B_{nlm}$, and $C_{\nu\lambda\mu}$ is the primary observational task, while the determination of the three operator matrices $S$, $T$, and $U$ is the fundamental theoretical problem of sunspot seismology. Its solution presently hinges upon finding an effective means to connect the inner and outer expansions across the sunspot penumbra.

## 3. THE CROSS-CORRELATION FUNCTION

The time-distance sunspot seismology method introduced by Duvall et al. (1996) is based on cross-correlations of time series of the oscillations. The goal of this section is to determine how this correlation function depends upon the specification of the wave field developed in the § 2. To this end we may follow Braun (1997) in defining the center-annulus cross-correlation function by

$$C_0(\Delta, \tau) \equiv \frac{1}{T} \int_0^T dt\, \Psi(0, t)\Psi(\Delta, t + \tau)\,, \tag{7}$$

where $T$ is the duration of the observations and

$$\Psi(\theta, t) = \frac{1}{2\pi}\, \hat{\boldsymbol{e}}_r \cdot \frac{\partial}{\partial t} \int_{-\pi}^{\pi} d\phi\, \delta \boldsymbol{r}(r, \theta, \phi, t)\bigg|_{r = R_\odot}\,, \tag{8}$$

if, for example, the oscillation measurements are radial Doppler velocities. Because the time-distance methods are traditionally applied to azimuthally averaged quantities, only the $m = 0$ components of the wave field generally survive the angle-averaging integral that appears in equation (8).

It is a straightforward but somewhat tedious exercise to substitute the inner and outer expansions of § 2 into equations (7) and (8), and then to make use of equations (4) and (6) to eliminate the amplitudes $B_{nlm}$ and $C_{\nu\lambda\mu}$ in favor of the $S$-, $T$-, and $U$-matrices and the fundamental excitation amplitudes $A_{nlm}$ and $A_{\nu\lambda\mu}$. The resulting expression is found to involve several nested sums of terms that contain products of $A_{nlm}$ and $A_{\nu\lambda\mu}$. It may be argued on purely theoretical grounds that many of these terms will not make any sensible contribution to the center-annulus cross-correlation function. First, it is quite reasonable to assume that there are no statistical correlations between the various fundamental-mode amplitudes $A_{nlm}$ and $A_{\nu\lambda\mu}$, and so we may discard all terms from the nested sums except those that contain products of a particular amplitude with itself, i.e., $|A_{nlm}|^2$ and $|A_{\nu\lambda\mu}|^2$. Second, the time integration that appears in equation (7) will suppress all terms except those that satisfy $|\,\mathrm{Im}\,(\omega_{\nu\lambda})| \ll T^{-1}$ and $|\,\mathrm{Re}\,(\omega_{\nu\lambda}) - \omega_{nl}| \ll T^{-1}$. This follows from the fact that every term in the nested sums contains a factor of the form

$$\frac{1}{T} \int_0^T dt e^{(\pm i\omega_{nl} \pm i\omega_{\nu\lambda} - \Gamma_{\nu\lambda})t} = \frac{1}{T(\Gamma_{\nu\lambda} \mp i\omega_{nl} \mp i\omega_{\nu\lambda})} \times [1 - e^{(\pm i\omega_{nl} \pm i\omega_{\nu\lambda} - \Gamma_{\nu\lambda})T}]\,, \tag{9}$$

where we have let $\Gamma_{\nu\lambda} = \mathrm{Im}\,(\omega_{\nu\lambda})$ and $\omega_{\nu\lambda} = \mathrm{Re}\,(\omega_{\nu\lambda})$ in order to make explicit the manner in which the damping of the internal umbral oscillations affects the center-annulus cross-correlation function.

With these appropriate terms omitted, we find that $C_0(\Delta, \tau)$ can be partitioned into two separate contributions that arise from the induced and spontaneous $p$-mode emission processes,

$$C_0(\Delta, \tau) = C_0^{\rm ind}(\Delta, \tau) + C_0^{\rm spn}(\Delta, \tau) . \quad (10)$$

The explicit forms of these two contributions are

$$C_0^{\rm spn}(\Delta, \tau) = \tfrac{1}{2}{\rm Re}\left\{\sum_{nl\nu\lambda}{}' c_{\nu\lambda}^{nl} e^{i\omega_{nl}\tau}[Y_{l0}^{(+)}(\Delta)\mathscr{T}_{nl0}^{\nu\lambda 0} \mid A_{\nu\lambda 0}\mid^2]\right\} \quad (11)$$

and

$$C_0^{\rm ind}(\Delta, \tau) = \tfrac{1}{2}\ {\rm Re}\left\{\sum_{nl\nu\lambda}{}' c_{\nu\lambda}^{nl} e^{i\omega_{nl}\tau}[Y_{l0}^{(-)}(\Delta)\overline{\mathscr{U}_{\nu\lambda 0}^{nl0}} \mid A_{nl0}\mid^2 + Y_{l0}^{(+)}(\Delta)\sum_{n'l'm'}\overline{\mathscr{U}_{\nu\lambda 0}^{n'l'm'}}\mathscr{S}_{nl0}^{n'l'm'} \mid A_{n'l'm'}\mid^2]\right\}, \quad (12)$$

where the coefficients $c_{\nu\lambda}^{nl}$ are defined by

$$c_{\nu\lambda}^{nl} \equiv \omega_{\nu\lambda}\,\omega_{nl}\,\overline{\xi_{\nu\lambda}^{<}(R_\odot)}\xi_{nl}^{>}(R_\odot)\overline{Y_\lambda^0(0)} . \quad (13)$$

We have implicitly assumed that practical complications associated with different heights of formation of Fraunhofer lines in sunspots and quiet Sun, as well as contingencies required to deal with the juxtaposition of magnetized and unmagnetized radiating atmospheres, are accounted for through the $\xi_{\nu\lambda}^{<}(R_\odot)$ factor that appears in equation (13). Finally, we remark that the prime on the outermost sums of equations (11) and (12) signifies that the indices are restricted to those values for which Im $(\omega_{\nu\lambda}) = 0$ and Re $(\omega_{\nu\lambda}) = \omega_{nl}$, and the overline is employed to denote complex conjugation.

The above four equations are the desired outcome of our efforts in this section. In § 4 we evaluate these expressions based on the recent measurements made by Braun (1997), but before doing so, we find it worthwhile to pause and make several observations regarding the content of these equations. Both the spontaneous and induced emission contributions to the center-annulus cross-correlation function result in the superposition of a large number of complex numbers, which for the most part have no definite phase relationship. The dominant contribution to the sum therefore arises from the small subset of these terms in which their phases are nearly aligned. That such subsets must indeed be present may be appreciated by noting that

$$\arg\,[Y_{l0}^{(\pm)}(\Delta)] \approx \mp\left[\left(l+\frac{1}{2}\right)\Delta - \frac{\pi}{4}\right] \quad (14)$$

for sufficiently large $l$ and $\Delta$ bounded away from 0 and $\pi$ (Abramowitz & Stegun 1964, p. 336). Since the solar acoustic oscillations have $\omega_{nl} \propto l^{0.3-0.5}$, it follows that for every fixed positive $\Delta$, there exists along each $p$-mode ridge a point of stationary phase[6] at $l \approx l_n(\Delta, \tau)$. Since $l_n$ must be a positive real number, the terms that contain the $Y_{l0}^{(-)}(\Delta)$ factor have stationary phase points for negative values of the time lag $\tau$, while the terms containing $Y_{l0}^{(+)}(\Delta)$ have stationary phase points for positive values of $\tau$. The further requirement that the contributions from the stationary phase points along individual $p$-mode ridges add coherently selects a specific negative $\tau = -\tau^-(\Delta)$ (for terms with $Y_{l0}^{(-)}$ factors) and positive $\tau = \tau^+(\Delta)$ (for terms with $Y_{l0}^{(+)}$ factors) correlation time for each value of $\Delta$. Hence, the spontaneous emission of $p$-modes within the sunspot and mode mixing of the incoming and outgoing $p$-modes influence only the outgoing $\tau^+$ correlation time and leave the incoming $\tau^-$ correlation time unaffected.

In applying equations (10), (11), (12), and (13) to the analysis of a quiet-Sun control experiment, one may assume that $\mathscr{S}_{nlm}^{n'l'm'} = \mathscr{U}_{\nu\lambda\mu}^{n'l'm'} = \delta_{n',n}\,\delta_{l',l}\,\delta_{m',m}$ (where these $\delta$'s are Kronecker $\delta$'s) and neglect the contribution of the spontaneous emission term, $C_0^{\rm spn}(\Delta, \tau)$, to obtain

$$C_0(\Delta, \tau) = C_0^{\rm ind}(\Delta, \tau) = \sum_{nl}\omega_{nl}^2 \mid \xi_{nl}^{>}(R_\odot)A_{nl0}\mid^2 Y_l(0)Y_l(\Delta)\cos\,\omega_{nl}\tau , \quad (15)$$

a result that has been previously obtained by Kosovichev & Duvall (1998). Any deviation of the measured quiet Sun $C_0(\Delta, \tau)$ from this prediction is therefore indicative of significant acoustic emission within the region $0 \le \theta \le \theta_>$, which is accounted for by $C_0^{\rm spn}(\Delta, \tau)$, and/or the presence of nearby coherent sources leading to correlations between distinct $A_{nlm}$.

We conclude this section by remarking that the quiet-Sun center-annulus cross-correlation function is invariant under time reversal $\tau \to -\tau$, and consequently it can exhibit no time asymmetries between its negative and positive correlation times; i.e., $\delta\tau = 0$. This time-reversal symmetry is present because the product of the coefficient $c_{\nu\lambda}^{nl}$ and the quantity enclosed by square brackets in equation (12) is a real number for conditions that pertain to the quiet-Sun control experiment.[7] Woodard (1997) has demonstrated that wave dissipation must break the time-reversal symmetry and cause $\delta\tau \neq 0$. Mode conversion between the fast and slow magnetoatmospheric wave modes in the sunspot umbra, for example, leads to complex umbral oscillation eigenfunctions $\xi_{\nu\lambda}^{<}(r)Y_\lambda^0(\theta)$. This will naturally produce complex values for the coefficients $c_{\nu\lambda}^{nl}$ and the $U$- and $S$-matrices that will generate nonzero time asymmetries in agreement with Woodard's findings. Equation (11) indicates that spontaneous emission of $p$-modes by stresses within the sunspot can also create time asymmetries in the center-annulus cross-correlation function.

## 4. NOAA 7912: TIME-DISTANCE VERSUS FREQUENCY-WAVENUMBER

The theoretical developments of §§ 2 and 3 imply an explicit relationship between the $S$-matrix concepts of frequency-wavenumber helioseismology and the center-annulus cross-correlation function of time-distance helioseismology. The goal of the present section is to determine to what extent these relationships are corroborated by actual helioseismic data. To this end, we shall utilize GONG data pertaining to the 1995 October 11–20 disk passage of the active region NOAA 7912, data which have recently been analyzed by Braun (1997).

In Braun (1997), this active region and several others are studied using time-distance methods, and the reader should consult this paper for a thorough discussion of their implementation. To facilitate our comparison of the two approaches, it is first necessary to reanalyze these same data

[6] A point of stationary phase nominally occurs where $\partial/\partial l$ of arg $[Y_{l0}^{(\pm)}(\Delta)\exp(i\omega_{nl}\tau)]$ vanishes. Of course, the precise location of the stationary phase point may also depend in part upon $l$ dependences of the $S$-, $T$-, and $U$-matrices.

[7] Note that $\overline{Y_{lm}^{(\pm)}(\Delta)} = Y_{lm}^{(\mp)}(\Delta)$ for real values of $l$, $m$, and $\Delta$.

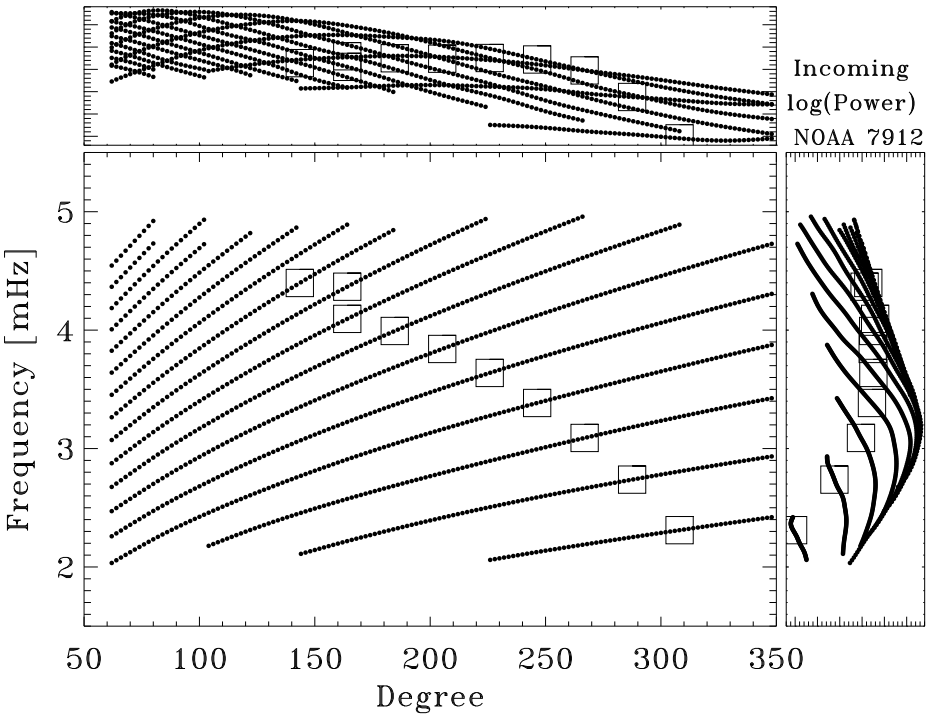


FIG. 2.—The *l*-*v* diagram for the incoming wave field for active region NOAA 7912 as determined by data from the GONG instruments. The side panels show the projection of the logarithm of the mode power (in arbitrary units) along the frequency and spherical harmonic degree axes. The lowest ridge corresponds to $n = 1$. The squares overplotted on several ridges show the approximate location of the peak absorption along that ridge (see Fig. 3).

using the frequency-wavenumber approach as outlined by Braun (1995). We pause briefly to present the results of this (re)analysis before proceeding with our computations.

Figure 2 shows the portion of the *l*-*v* diagram[8] used to effect the Fourier-Bessel decomposition of the wave field in the outer annulus, $2\overset{\circ}{.}5 \leq \theta \leq 30^\circ$. The two side panels show the projection of the measured incoming wave power, $P_{nl} \equiv |\omega_{nl}\xi^{>}_{nl}(R_\odot)A_{nl0}|^2$, along the frequency and spherical harmonic degree axes for the $T = 204.8$ hr duration of the observations. These amplitudes are reckoned using Hankel functions, $H_0^{(1,2)}(L\theta)$, where $L = [l(l+1)]^{1/2}$, in lieu of the propagating spherical harmonics $Y_{l0}^{(\pm)}(\theta)$. As noted by Braun (1995), this approximation is not likely to lead to errors greater than a fraction of a percent in the present application to *p*-modes with $m = 0$.

In Figure 3, the derived absorption coefficients and phase shifts,

$$\alpha_{nl} = 1 - \left\langle \frac{|B_{nl}|^2}{|A_{nl}|^2} \right\rangle \quad \text{and} \quad \delta_{nl} = \left\langle \arg\left(\frac{B_{nl}}{A_{nl}}\right) \right\rangle, \quad (16)$$

(see eqs. [1] and [5]) are plotted along with selected 1 $\sigma$ error bars. As discussed by Braun (1995), these quantities are in fact coarse-grained averages over spherical harmonic degree bins of $\Delta l \approx 20$ and over several azimuthal orders *m*, assuming that the actual quantities vary slowly over this range of mode parameters. Because the incoming wave amplitudes result from a particular realization of the stochastic excitation of *p*-modes by turbulent convection, the individual arg $[A_{nl}(\nu)]$ and arg $[B_{nl}(\nu)]$ fluctuate dramatically from point to point across the *l*-*v* diagram. As a result of instrumental noise, spontaneous emission, and mode mixing, even fluctuations in their differences are in no sense inconsequential, and so it is imperative to build the signal-to-noise ratio by averaging these differences over a small but finite range of values for $\nu$, *l*, and *m*. It is the result of such an averaging process that is displayed in Figure 3.

The general features of these plots are in good overall quantitative agreement with the previous findings of Braun (1995) for active regions NOAA 5254 and 5229, which were observed for 2 weeks during 1988 November from the geographic South Pole (Braun et al. 1992). The upper panel indicates a quadratic $\delta \propto \omega^2$ dependence of the phase shift on the mode frequency, with the largest phase shifts obtained for modes with the lowest radial orders. The lower panel shows the tendency for the absorption along each ridge to peak at successively greater frequencies as the radial order increases. This behavior is further emphasized in Figure 2 by overplotting boxes at the approximate locations of the peak absorption along each ridge in the *l*-*v* diagram.

It is more difficult to determine the off-diagonal elements of the *S*-matrix, and it is harder still to distinguish the spontaneous emission of *p*-modes within the spot from instrumental noise in the Dopplergrams. For the South Pole observations, Braun (1995) estimated that the mode mixing between adjacent *p*-mode ridges probably does not exceed $\approx 10\%$, and he found evidence for substantial $\approx 100^\circ$–$200^\circ$ phase shifts for the off-diagonal elements of the *S*-matrix. Similar results are likely to apply to NOAA 7912, but in view of the prohibitive computational expense and uncertain nature of the outcome of such an endeavor, we will not attempt to go beyond the basic determination of the diagonal of the *S*-matrix as shown in Figure 3.

### 4.1. *The Quiet Sun*

As a prelude to tackling the comparative study for active region NOAA 7912, Figures 4 and 5 show that excellent

[8] In this section, $\nu$ will generally be used to denote the cyclic frequency of the solar acoustic oscillations and should not be confused with the radial order $\nu$ of the internal umbral oscillation eigenfunctions discussed in § 3.

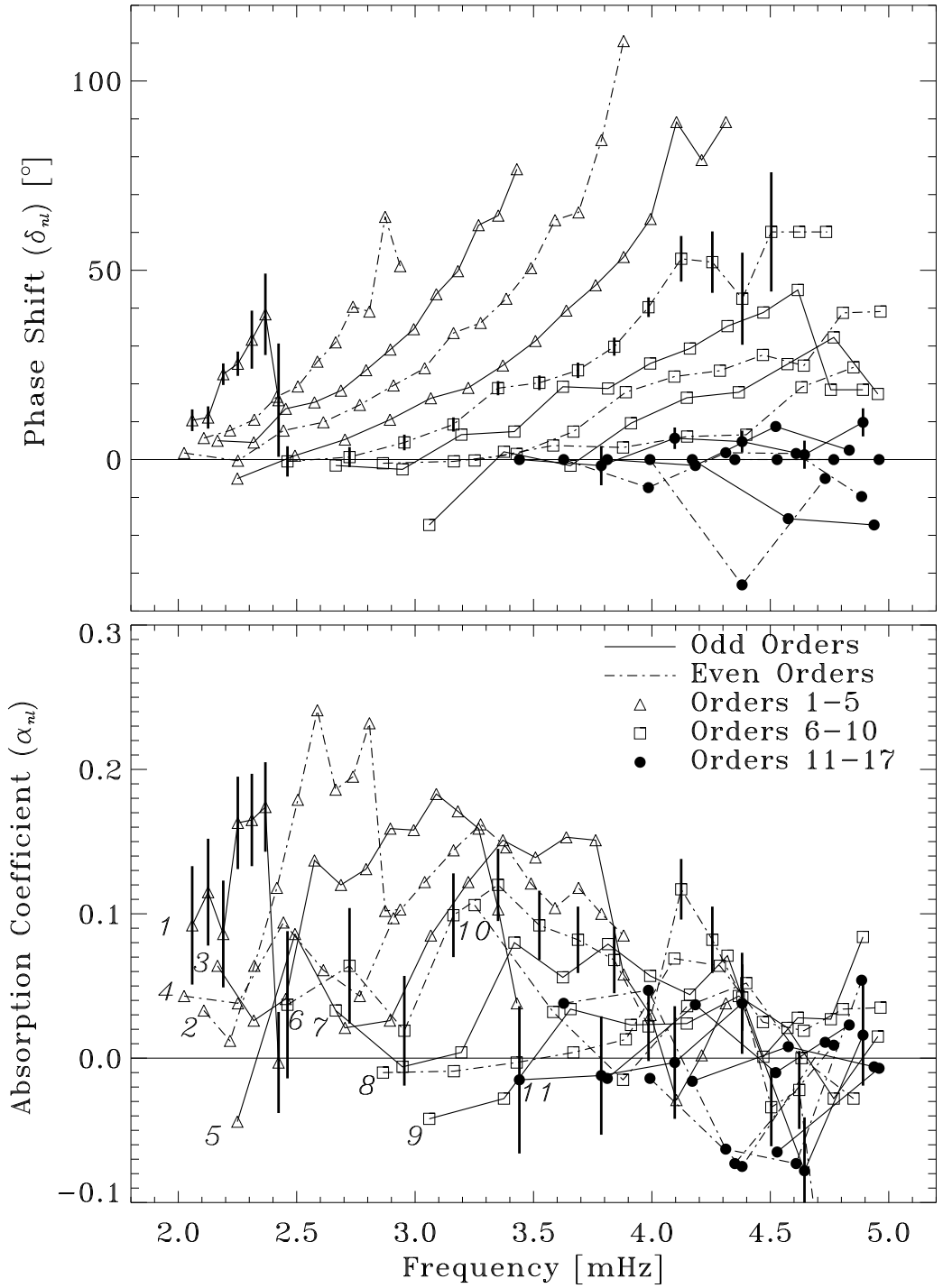


FIG. 3.—Plot of the derived phase shifts (*upper panel*) and absorption coefficients (*lower panel*) for active region NOAA 7912. Representative 1 $\sigma$ error bars are shown only for the $n = 1$, 6, and 11 ridges to avoid excessive clutter. In the lower panel, the $n = 1, 2, \ldots, 11$ ridges are explicitly labeled.

agreement between the simulated and observed center-annulus cross-correlation function is readily obtained for the quiet-Sun reference region. The right-hand panel of Figure 4 shows a gray-scale rendering of $C_0(\Delta, \tau)$ measured by Braun (1997) using GONG data. Three curved bands of enhanced correlation are clearly visible in this plot. In the ray-path formulation of time-distance helioseismology, these bands are identified with the first, second, and third skips of the ray bundle from the solar surface. The left-hand panel of this figure shows the corresponding construction of $C_0(\Delta, \tau)$ based on equation (15). This result is obtained by summing the $\approx 1300$ individual modes whose frequencies $\nu_{nl}$ and power levels $P_{nl}$ are indicated by the filled circles plotted in Figure 2. The *p*-modes summed in equation (15) suffer no dissipation, and no noise has been added to the simulated cross-correlation function; consequently, the synthetic time-distance diagram is crisper in appearance and shows an additional fourth skip that is absent in the observations.

A further quantitative comparison of the simulated and observed center-annulus cross-correlation functions is afforded by Figure 5. There, following Braun (1997), the

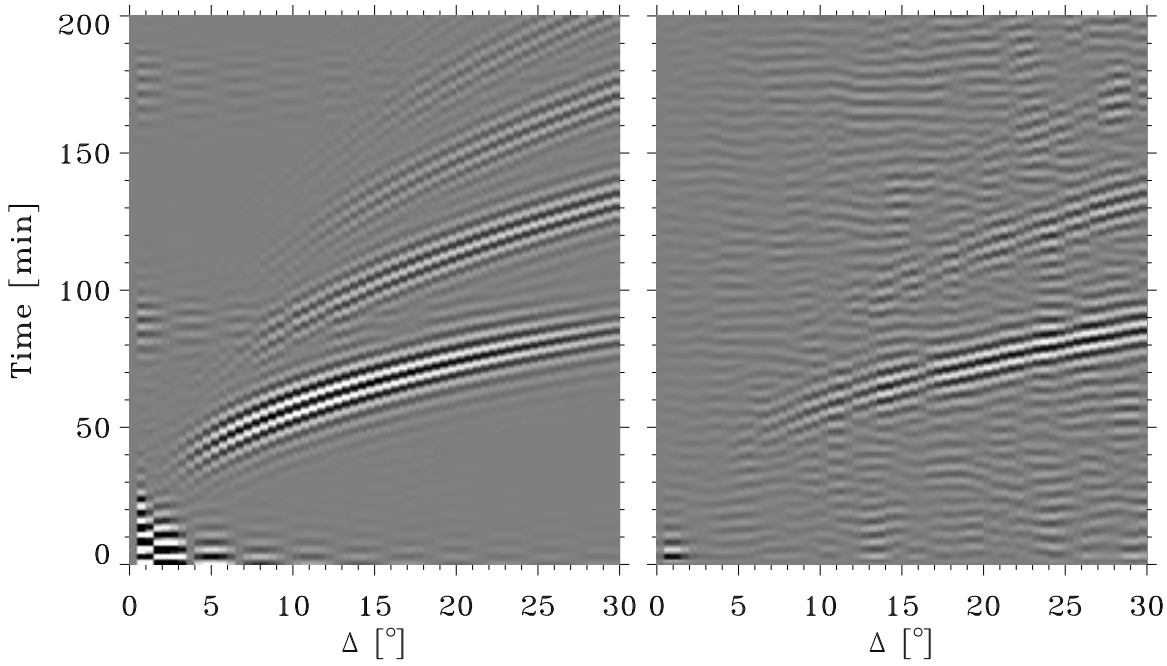


FIG. 4.—Relief plot of the center-annulus cross-correlation function $C_0(\Delta, \tau)$ as a function of annular polar angle ($\Delta$) and positive time lag ($\tau$). The left-hand panel is the simulated result obtained by using the mode frequencies and amplitudes plotted in Fig. 3 to evaluate eq. (15). The right-hand panel is the analogous result computed by Braun (1997) using GONG data for the quiet-Sun reference region.

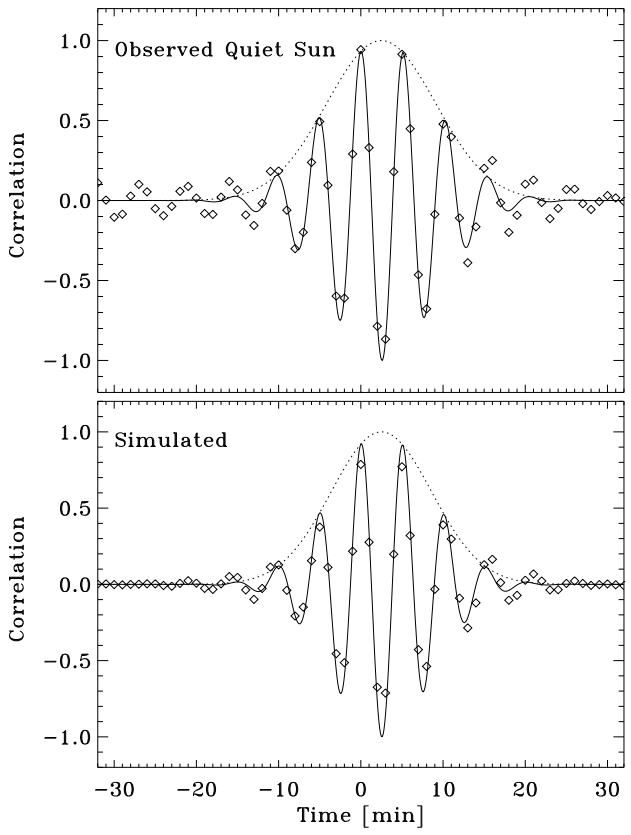


FIG. 5.—First-skip correlations of Fig. 4, shifted in time and summed over the range $5° \leq \Delta \leq 25°$, are plotted as diamonds for the observations (*upper panel*) and the simulated (*lower panel*) quiet-Sun center-annulus cross-correlation functions. The solid curves are distinct Gabor wavelet fits (see eq. [17]) to the observed and simulated data, and the dotted curves are the exponential envelopes of these wavelets. Time = 0 corresponds to the mean correlation time for the quiet-Sun reference region $\bar{\tau}_{qsr}(\Delta)$ determined by Braun (1997).

first-skip correlations over a range of $\Delta$ from 10° to 25° are shifted in time and summed to increase the signal-to-noise ratio. Both the real and simulated correlations (*diamonds*) are fit by a Gabor wavelet,

$$G(A, \omega_0, \sigma, \tau_{ph}, \tau_{en}; \tau) = A \cos [\omega_0(\tau - \tau_{ph})] \exp \left[ -\left( \frac{\tau - \tau_{en}}{\sqrt{2}\sigma} \right)^2 \right], \quad (17)$$

with five parameters, $A$, $\omega_0$, $\sigma$, $\tau_{ph}$, and $\tau_{en}$. The solid curves plotted in the upper and lower panels of Figure 5 are the full Gabor wavelet fits, while the dashed curves show only the exponential envelopes. The excellent agreement between theory and observation is once again apparent.

### 4.2. *Active Region NOAA 7912*

The chief difficulties encountered in repeating the success of § 4.1 for NOAA 7912 are a lack of information on both the $U$-matrix and the off-diagonal elements of the $S$-matrix, coupled with complete ignorance of the spontaneous $p$-mode emission within the sunspot. The center-annulus cross-correlation function contains information on these quantities that is not easy (e.g., the off-diagonal components of the $S$-matrix), or even possible (e.g., the umbral oscillation spectrum), to determine with the traditional frequency-wavenumber methods. In this regard, the investigations of Abdelatif, Lites, & Thomas (1986) and Penn & LaBonte (1993), in which attempts were made to determine an $l$-$\nu$ diagram for the umbra of a sunspot, are indicative of the required extension of the frequency-wavenumber approach that is necessary to sharpen the analysis techniques.

In lieu of attempting a direct synthetic prediction of the sunspot center-annulus cross-correlation function based on equations (10), (11), (12), and (13), we instead focus our

attention on establishing a sense of how phase shifts and absorption coefficients influence the determination of the phase and envelope times $\tau_{\rm ph}^{\pm}$ and $\tau_{\rm en}^{\pm}$. To this end, we compute $C_0^{\rm ind}(\Delta, \tau)$ using equation (12), and, assuming that $\mathscr{S}_{nl}^{n'l'} = \delta_{n,n'}\delta_{l,l'}(1-\alpha_{nl})^{1/2}\exp(i\delta_{nl})$ and $\mathscr{U}_{\nu\lambda}^{n'l'} = \delta_{\nu,n'}\delta_{\lambda,l'}\exp[i(\frac{1}{2}\delta_{nl}-\varphi)]$, where $\varphi$ is a constant phase retardance. As before, the summation is carried out over the $\approx$1300 modes displayed in Figure 2, with the absorption coefficients ($\alpha_{nl}$) and phase shifts ($\delta_{nl}$) interpolated from the measurements presented in Figure 3 and the frequencies $\omega_{nl}$ and power levels $P_{nl}$ taken from Figure 2. The phase retardance $\varphi$ is set to 0.5 rad ($\approx 28\overset{\circ}{.}6$) for reasons that will be discussed shortly. In Figure 6, the resulting mean $\bar{\tau} = \frac{1}{2}(\tau_{\rm ph}^{+} + \tau_{\rm ph}^{-})$ and difference $\delta\tau = \tau_{\rm ph}^{+} - \tau_{\rm ph}^{-}$ phase times determined from the Gabor wavelet fits are plotted as functions of the annular polar angle $\Delta$. Also plotted for reference are the analogous simulated results for the quiet Sun (*dashed lines*), as well as measurements for the quiet-Sun reference region (Braun 1997; *open circles*) and NOAA 7912 (*filled circles*).

The slight decrease of $\bar{\tau}$ from the quiet-Sun reference value is a consequence of the positive phase shifts of the outgoing waves (Fig. 3). The tendency for these phase shifts to increase with increasing spherical harmonic degree is mirrored in the corresponding decrease in the mean travel time offset with increasing annular size. As previously noted by Braun (1997), the measured phase shifts $\delta_{nl}$ are too small to account for the observed $\bar{\tau}$ discrepancy between NOAA 7912 and the quiet Sun, but they are consistent[9] with the predictions plotted in the lower panel of Figure 6. To reproduce the observed $\bar{\tau}$ for NOAA 7912 would require mean phase shifts approaching 50°, which is clearly at odds with the data plotted in the upper panel of Figure 3. Although they are significantly noisier, the pure $m = 0$ phase shifts do tend to be about 30%–50% larger than the $m$-averaged values plotted in Figure 3 (see Fig. 12 of Braun 1995), and the phase advances of the off-diagonal mode-mixing components of the $S$-matrix are likely to be in the range of 100°–200°. So we suspect that our inability to reproduce the observed $\bar{\tau}$ is most likely a consequence of significant mode mixing, coupled with an underestimation of the true $\delta_{nl}$, although we cannot rule out the possibility that significant $p$-mode emission is occurring within the spot.

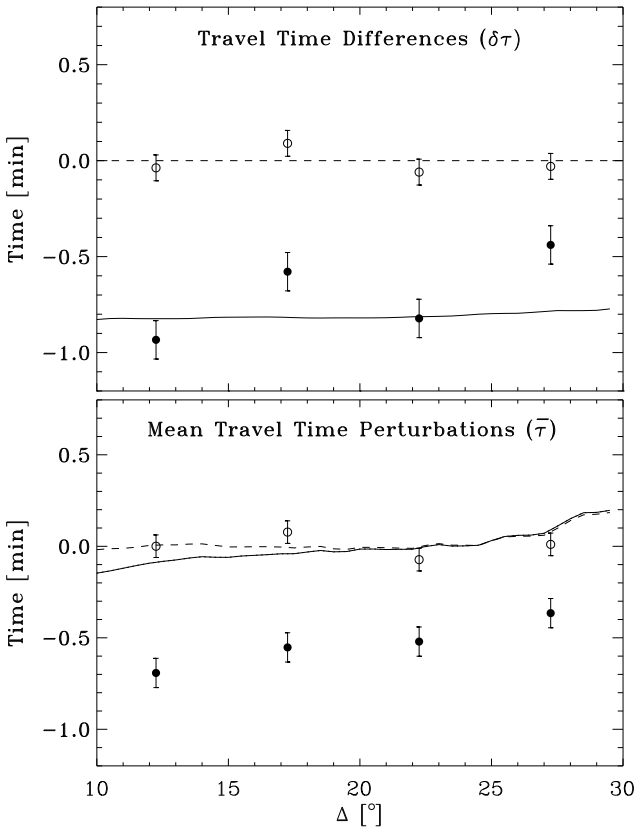


FIG. 6.—Mean anomalies $\bar{\tau} - \bar{\tau}_{\rm qsr}$ (*lower panel*), where $\bar{\tau}_{\rm qsr}(\Delta)$ is the mean correlation time for the quiet-Sun reference region, and differences (*upper panel*) of the incoming and outgoing phase correlation times are plotted as functions of the annular polar angle $\Delta$. The solid and dashed lines result from the simulations for NOAA 7912 and the quiet Sun, respectively, based on the formulae derived in §§ 2 and 3. The open and filled symbols are the analogous observational results for the quiet-Sun reference region and NOAA 7912, respectively, published by Braun (1997).

On the other hand, Figure 6 indicates that our naive estimate of $C_0^{\rm ind}(\Delta, \tau)$ does a remarkably good job at reproducing the observed time difference $\delta\tau$ for NOAA 7912. This good fortune is entirely attributable to the $\varphi = 0.5$ rad phase lag imposed on the umbral oscillations. Of course, the actual phase relationship between the umbral oscillations and incoming $p$-modes is not known to us, so our working hypothesis was to apportion half the measured total phase shift $\delta_{nl}$ and then subtract 0.5 rad. This prescription is based on the notion that the spot might behave somewhat like an elastic scatterer given the relatively modest values of the absorption coefficients plotted in the lower panel of Figure 2. The additional action of subtracting a constant phase lag is motivated by some crucial insight gained from high spatial and temporal resolution observations of the umbral oscillations, which we now describe.

Observations of NOAA 7912 were recorded with the HAO/NSO Advanced Stokes Polarimeter (Elmore et al. 1992; Skumanich et al. 1997) at the Vacuum Tower Telescope at the NSO/Sacramento Peak on 1995 October 15. A comprehensive discussion of these observations and the instrumental setup will be provided elsewhere (Lites et al. 1998). For our present purposes, it suffices to mention that the spectrograph slit of width $0\overset{''}{.}37$ was placed across the center of the sunspot and that observations were made with a 9.91 s cadence between UT 14:29 and UT 16:38. At each spatial location along the slit, the ASP records the full $I$, $Q$, $U$, and $V$ components of the Stokes vector over a wavelength range of $\approx$0.5 nm, which includes the Zeeman-sensitive lines Fe I 630.15 nm and 630.25 nm, as well as the Ti I 630.4 nm line. The wavelength resolution of the recorded spectrum is 1.26 pm pixel$^{-1}$. At each temporal and spatial location, the full $I$, $Q$, $U$, and $V$ line profiles of the Fe I 630.15 nm and 630.25 nm absorption features are subjected to an inversion based on the Milne-Eddington solution of the Unno-Rachkovsky equations of plane-parallel magnetized radiative transfer. This operation yields inferred values of the (instantaneous) magnetic field strength and orientation as well as the line-of-sight velocity and assorted atmospheric thermodynamic parameters (Jefferies, Lites, & Skumanich 1989).

Only the time series of the line-of-sight component of the fluid motion are germane to our present discussion. The left-hand panel of Figure 7 shows the cross-correlation of the Doppler velocity-time series determined from the inversion of the Stokes profiles. The cross-correlation is com-

[9] A time deficit of 0.15 minutes corresponds to a positive phase shift of about 11° for an oscillation with a period of 5 minutes.

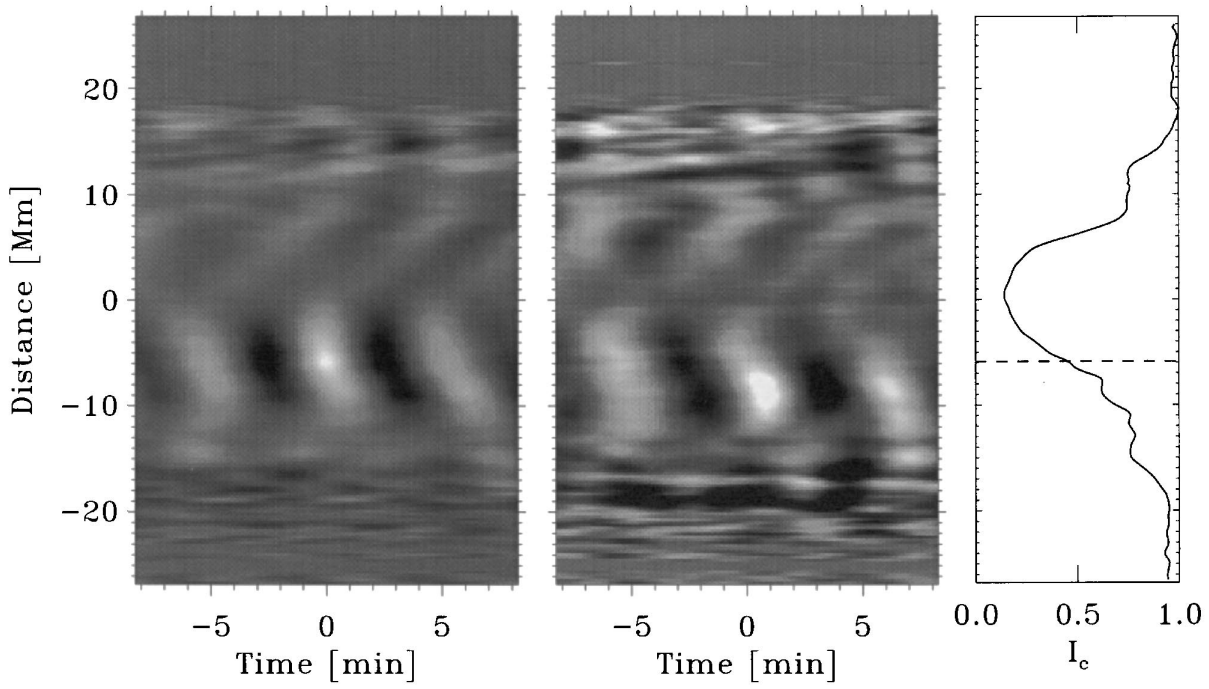


FIG. 7.—Relief plot of the cross-correlation of the Doppler velocities at different spatial locations across NOAA 7912 (*ordinate*) obtained with the HAO/NSO Advanced Stokes Polarimeter (ASP) and offset by a time $\tau$ (*abscissa*), with the ASP time series $-6$ Mm from the spot center (*left-hand panel*) and the GONG Doppler time series (*center panel*). For reference, the mean profile of the continuum intensity across the spot at 630 nm is displayed in the right-hand panel, and the overplotted dashed line indicates the location of the largest correlation between the GONG and ASP Doppler time series at zero time lag.

puted between the Doppler velocity at each position along the slit (separated by 0.″37) and the Doppler velocity at a position near the inner boundary of the penumbra, approximately 6 Mm distant from the center of the spot. A characteristic "herringbone" pattern with a predominant 5 minute period is clearly visible in the cross correlation of the ASP time series, a property of umbral oscillations that was previously noted by Thomas, Cram, & Nye (1984). It is also apparent that the oscillations exhibit a phase lag relative to the center of the umbra that increases with distance from the spot center. At distances as large as 10 Mm from the center of the umbra, the oscillations lag those observed in the center of the umbra by more than 2 minutes. The middle panel of Figure 7 shows in an analogous format the cross-correlation computed between the ASP Doppler velocity-time series and the GONG Doppler velocity-time series measured in the wings of the Ni I 676.8 nm line. Special care has been taken to assure that there are no spurious time offsets between the ASP and GONG time series. The spatial registration of the two data sets is more problematic given that the ASP pixels are 0.″37 on a side while the analogous GONG pixels are almost a factor of 20 larger (8.″5 × 10.″9).

In any case, the point to appreciate from this panel is that the GONG signal correlates best with the ASP oscillations about 6 Mm distant from the umbral center, near the inner boundary of the penumbra. Here the continuum intensity is a factor of 3 larger than that of the umbral center and the ASP-inferred magnetic field strength is about 66% of its peak value in the center of the umbra. At a distance of 6 Mm from the center of this spot, the magnetic field is inclined about 30° with respect to the local vertical. However, the key point we wish to stress is that the oscillation signal 6 Mm from the center of this sunspot lags the oscillations on the umbral axis by 30–50 s. This time lag is clearly of the same sense and magnitude as the time differences reported by Duvall et al. (1996) and Braun (1997). Figure 7 therefore argues strongly that the observed $\Psi(0, t)$ is contaminated by oscillation signals originating from the inner boundary of the sunspot penumbra, and this in turn introduces a spurious phase lag of $\approx 0.5$ rad to the supposed GONG umbral oscillation time series because of the "herringbone" character of the umbral 5 minute oscillations. This point is nicely confirmed by Figure 6, which shows substantial agreement between the simulated and observed time differences $\delta\tau$ when the umbral signal is artificially lagged by $\varphi = 0.5$ rad with respect to its presumed phase of $\frac{1}{2}\delta_{nl}$. The fact that the simulated center-annulus cross-correlation function for NOAA 7912 predicts an erroneous $\bar{\tau}$ (and consequently incorrect values for the individual $\tau^-$ and $\tau^+$) is evidence that our ad hoc prescription for the umbral phase lag of $\frac{1}{2}\delta_{nl}$ is in error. This comes as no surprise given our general ignorance of the $U$-matrix.

## 5. CONCLUSION

A recapitulation of the developments set forth in the previous three sections begins with the recognition that equations (10), (11), (12), and (13) provide, for the first time, a rigorous connection between the measured quantities and concepts employed by the time-distance and frequency-wavenumber formulations of local helioseismology without recourse to the eikonal approximation. Although these formulae do not immediately lend themselves to transparent physical interpretations, they nevertheless offer valuable insight into the manner in which mode mixing, spontaneous $p$-mode emission, and the peculiar character of the umbral oscillations can affect the center-annulus cross-correlation function. Through the exercise of applying these formulae to the GONG observations of active region NOAA 7912 previously analyzed by Braun (1997), we are able to demon-

strate that spurious time lags of the umbral oscillation produce time differences $\delta\tau$ while leaving the mean correlation time $\bar{\tau}$ unaffected, while, conversely, mode mixing and spontaneous $p$-mode emission from within the sunspot affect only the outgoing correlation time $\tau^+$, and therefore impact both $\delta\tau$ and $\bar{\tau}$. By combining GONG and simultaneous ASP observations, we were further able to deduce that penumbral contamination coupled with the characteristic herringbone pattern of 5 minute oscillations in sunspots leads to a spurious phase lag of the "umbral oscillation signal" in observations with insufficient spatial resolution. This phase lag is manifested as a correlation time difference $\delta\tau$ of the sign and magnitude previously reported by Duvall et al. (1996) and by Braun (1997). Consequently, the interpretation advanced by Duvall et al. (1996) that this observed time difference is evidence for steady downflows within the spot and its immediate vicinity must be viewed with some skepticism.

The deliberations of § 4 suggest that the use of time-distance and frequency-wavenumber concepts in concert, along with spatially resolved observations both outside and within (Abdelatif et al. 1986; Penn & LaBonte 1993) the spot, has the potential to drastically enhance the diagnostic capabilities of either of these approaches pursued in isolation. In the present investigation, a rather coherent and satisfying picture of the interaction of the solar acoustic oscillations with an isolated sunspot begins to emerge. The forcing of the sunspot below the visible solar surface by the incoming acoustic wave field leads to the generation of magnetoatmospheric waves within the sunspot flux tube and results in the subsequent scattering and reemission of outwardly propagating $p$-modes in the surrounding quiet Sun. The upwardly propagating slow magnetoatmospheric wave modes, which are guided by the spot's magnetic field, emerge at first through the formation height of the Fe I 630.15 nm and 630.25 nm lines on the central axis of the umbra and then subsequently appear at progressively later times the further one looks from the axis of the spot. This results in the herringbone pattern shown in the left-hand panel of Figure 7. The apparent radial phase speed of this pattern is $\approx 100$ km s$^{-1}$, which is far greater than characteristic sound or Alfvén speeds at continuum optical depths between $10^{-2}$ and $10^{-1}$, at which these neutral iron lines are formed (Bruls, Lites, & Murphy 1991). The time lags shown in Figure 7 most likely result from a dispersion in (acoustic) propagation times between the $p$-mode forcing level and the height of formation of the iron lines, presumably a consequence of the greater path length of the inclined magnetic field lines joining the forcing and observing layers in the penumbra relative to the center of the umbra. These upwardly propagating waves not only lead to a suppression of the outwardly propagating $p$-modes, as evidenced by the absorption coefficients plotted in Figure 3, but because of the large continuum-intensity contrast across the spot (see Fig. 7, right-hand panel), they also induce a spurious phase delay in the unresolved umbral oscillation signal that results in the characteristic negative time difference $\delta\tau \approx 30$–$50$ s of the center-annulus cross-correlation function.

We thank Tim Brown and an anonymous referee for their insightful comments on an earlier version of this manuscript that led to a marked improvement in the clarity of exposition of the material presented in §§ 2 and 3. The GONG data were acquired by instruments operated by the Big Bear Solar Observatory, High Altitude Observatory, Learmouth Solar Observatory, Udaipur Solar Observatory, Instituto de Astrofisica de Canarias, and Cerro Tololo Inter-American Observatory. We are grateful to the observers at the NSO/Sacramento Peak Vacuum Tower Telescope, Steve Hegwer, Richard Mann, and Brian Armstrong, for their assistance with the ASP observations. The research of D. C. B. was supported by NSF grants AST-9496171, AST 95-21637, AST 95-28249, and ATM 92-14714. J. H. T. was supported by NASA grant NAGW-2123.

## REFERENCES

Abdelatif, T. E., Lites, B. W., & Thomas, J. H. 1986, ApJ, 311, 1015
Abdelatif, T. E., & Thomas, J. H. 1987, ApJ, 320, 884
Abramowitz, M., & Stegun, I. A. 1964, Handbook of Mathematical Functions (Washington, DC: National Bureau of Standards)
Bogdan, T. J. 1997, ApJ, 477, 475
Bogdan, T. J., Brown, T. M., Lites, B. W., & Thomas, J. H. 1993, ApJ, 406, 723
Bogdan, T. J., & Cally, P. S. 1995, ApJ, 453, 919
———. 1997, Proc. R. Soc. London A, 453, 943
Bogdan, T. J., Hindman, B. W., Cally, P. S., & Charbonneau, P. 1996, ApJ, 465, 406
Braun, D. C. 1995, ApJ, 451, 859
———. 1997, ApJ, 487, 447
Braun, D. C., Duvall, T. L., Jr., & LaBonte, B. J. 1988, ApJ, 335, 1015
Braun, D. C., Duvall, T. L., Jr., LaBonte, B. J., Jefferies, S. M., Harvey, J. W., & Pomerantz, M. A. 1992, ApJ, 391, L113
Braun, D. C., LaBonte, B. J., & Duvall, T. L., Jr. 1990, ApJ, 354, 372
Bruls, J. H. M. J., Lites, B. W., & Murphy, G. A. 1991, in Solar Polarimetry: Proc. 11th NSO/SP Summer Workshop, ed. L. J. November (Sunspot: NSO), 444
Cally, P. S. 1983, Sol. Phys., 88, 77
Cally, P. S., & Bogdan, T. J. 1993, ApJ, 402, 721
Cally, P. S., Bogdan, T. J., & Zweibel, E. G. 1994, ApJ, 437, 505
Chou, D.-Y., Chou, H.-Y., Hsieh, Y.-C., & Chen, C.-K. 1996, ApJ, 459, 792
Cox, J. P. 1980, Theory of Stellar Pulsation (Princeton: Princeton Univ. Press)
D'Silva, S., & Duvall, T. L., Jr. 1995, ApJ, 438, 454
D'Silva, S., Duvall, T. L., Jr., Jefferies, S. M., & Harvey, J. W. 1996, ApJ, 471, 1030
Duvall, T. L., Jr. 1995, in ASP Conf. Proc. 76, GONG 1994: Helio- and Astero-Seismology from the Earth and Space, ed. R. Ulrich, E. J. Rhodes, Jr., & W. Däppen (San Francisco: ASP), 465
Duvall, T. L., Jr., D'Silva, S., Jefferies, S. M., Harvey, J. W., & Schou, J. 1996, Nature, 379, 235
Duvall, T. L., Jr., Jefferies, S. M., Harvey, J. W., & Pomerantz, M. A. 1993, Nature, 362, 430
Duvall, T. L., Jr., et al. 1997, Sol. Phys., 170, 63
Elmore, D. F., et al. 1992, Proc. SPIE, 1746, 22
Fan, Y., Braun, D. C., & Chou, D.-Y. 1995, ApJ, 451, 877
Jefferies, J., Lites, B. W., & Skumanich, A. 1989, ApJ, 343, 920
Korzennik, S. G., Noyes, R. W., & Ziskin, V. 1995, in ASP Conf. Proc. 76, GONG 1994: Helio- and Astero-Seismology from the Earth and Space, ed. R. Ulrich, E. J. Rhodes, Jr., & W. Däppen (San Francisco: ASP), 268
Kosovichev, A. G. 1996, ApJ, 461, L55
Kosovichev, A. G., & Duvall, T. L., Jr. 1998, in Solar Convection and Oscillations and Their Relationship, ed. J. Christensen-Dalsgaard & F. Pijpers (Dordrecht: Kluwer), in press
Lebedev, N. N. 1972, Special Functions and Their Applications (New York: Dover)
Ledoux, P., & Walraven, T. 1958, Handbuch der Physik, ed. S. Flügge (New York: Springer), 353
Lites, B. W., Thomas, J. H., Bogdan, T. J., & Cally, P. S. 1998, ApJ, submitted
Parker, E. N. 1992, ApJ, 390, 290
Penn, M. J., & LaBonte, B. J. 1993, ApJ, 415, 383
Skumanich, A., Lites, B. W., Martínez Pillet, V., & Seagraves, P. 1997, ApJS, 110, 357
Spruit, H. C. 1991, in Lecture Notes in Physics 388, Challenges to Theories of the Structure of Moderate Mass Stars, ed. J. Toomre & D. O. Gough (Berlin: Springer), 121
Spruit, H. C., & Bogdan, T. J. 1992, ApJ, 391, L109
Thomas, J. H., Cram, L. E., & Nye, A. H. 1984, ApJ, 285, 368
Unno, W., Osaki, O., Ando, H., Saio, H., & Shibahashi, H. 1989, Nonradial Oscillations of Stars (Tokyo: Univ. Tokyo Press), 85
Woodard, M. F. 1997, ApJ, 485, 890